Ji Xu[a], Ting Liu[a], Hai Hu*, Yusheng Zhai, Ke Chen, Na Chen, Chi Li* and Xiaobing Zhang*

Design and optimization of tunneling photodetectors based on graphene/Al_2O_3/silicon heterostructures

Abstract

Recent discoveries in the field of graphene-based heterostructures have led to the demonstration of high-performance photodetectors. However, the studies to date have been largely limited to the heterojunction with a Schottky barrier, restricted by an inevitable compromise between photoresponsivity and photodetectivity. Here, a new class of graphene-based tunneling photodetectors is introduced by inserting the Al_2O_3 tunneling layer between silicon and graphene. The photocarriers can tunnel through the designed insulator layer which simultaneously blocks the dark current, thus maintaining high photodetectivity with desirable photoresponsivity. We further modulate the thickness of the Al_2O_3 layer to explore the tunneling mechanism for the photocarriers, in which a photoresponsivity of 0.75 A/W, a high current ratio of 4.8×10^3 and a photodetectivity of 3.1×10^{12} Jones are obtained at a 13.3-nm-thick Al_2O_3 layer. In addition, the fabrication process is compatible with conventional semiconductor processing, providing further flexibility to large-scale integrated photodetectors with high performance.

Keywords: Fowler-Nordheim theory; graphene; heterostructure; photoresponse; tunneling photodetector.

1 Introduction

Due to its unique structure, high carrier mobility and novel optical properties, graphene has been demonstrated as a promising material in optoelectronics that triggers extensive application prospect in photodetection [1–4]. Graphene-based photodetectors can provide high response speed over broadband spectral ranges [5–7], while exhibiting a relatively low responsivity owing to the 2.3% optical absorption [8]. In order to improve the responsivity, researchers tend to develop hybrid graphene with quantum dots [9, 10], plasmonic nanostructures [11, 12], waveguide [3, 13], or transition metal dichalcogenides (TMDCs) [14, 15], which enhances the light-matter interaction.

However, regardless of having a vertical or planar structure, the photodetectors are usually difficult to reconcile the contradiction between photoresponsivity and photodetectivity (mainly associated with the dark current), named as the trade-off effect [16]. For instance, an ultra-high on/off current ratio I_{ph}/I_{dark} (~10^5) is obtained from the MoS_2/graphene/MoS_2 heterostructure; the built-in barrier can lead to ultra-low dark current (<10^{-12} A) due to the photovoltaic effect, whereas the photoresponsivity is only ~0.03 A/W [17]. By contrast, a planar phototransistor based on graphene/Ti_2O_3 can acquire a high responsivity of 300 A/W as the trapped photogenerated carriers provide an additional electric field, while the photodetectivity falls to ~10^8 Jones [18]. As a result, it still remains a challenge to further achieve the best compromise between photoresponsivity and photodetectivity in the visible regime.

Recently, thin insulating films have been successfully employed as the tunneling layer in 2D-material-based photodetectors [19–21]. The introduction of the tunneling layer into vertical devices will not further complicate the

[a]**Ji Xu and Ting Liu:** This contributed equally to the work.
***Corresponding authors: Hai Hu and Chi Li,** Division of Nanophotonics, CAS Center for Excellence in Nanoscience, National Center for Nanoscience and Technology, Beijing 100190, China, e-mail: huh@nanoctr.cn (H. Hu); lichi@nanoctr.cn (C. Li). https://orcid.org/0000-0002-4243-2333 (H. Hu); and **Xiaobing Zhang,** Joint International Research Laboratory of Information Display and Visualization, Southeast University, Nanjing 210096, China, e-mail: bell@seu.edu.cn
Ji Xu: Joint International Research Laboratory of Information Display and Visualization, Southeast University, Nanjing 210096, China; and Division of Nanophotonics, CAS Center for Excellence in Nanoscience, National Center for Nanoscience and Technology, Beijing 100190, China
Ting Liu: National Institute for Materials Science, Tsukuba, Ibaraki 305-0044, Japan; and Institute of Materials and Systems for Sustainability, Nagoya University, Nagoya 4648601, Japan
Yusheng Zhai: Joint International Research Laboratory of Information Display and Visualization, Southeast University, Nanjing 210096, China
Ke Chen and Na Chen: Division of Nanophotonics, CAS Center for Excellence in Nanoscience, National Center for Nanoscience and Technology, Beijing 100190, China

structure or fabrication process. Meanwhile, similar to the effect of a traditional metal-insulator-semiconductor tunneling diode, the tunneling layer can effectively suppress the dark current between graphene and light absorber, thus, maintaining a desirable detectivity with an acceptable responsivity. In this work, we report a hybrid graphene/Al_2O_3/silicon tunneling photodetector in which the Al_2O_3 acts as the tunneling layer, while the photoexcitation residing in the silicon and graphene offers an efficient pathway as well as the collector for photocarriers. Under the illumination of 658 nm light, a responsivity of 0.75 A/W, a high current ratio of 4.8×10^3 and a detectivity of 3.1×10^{12} Jones have been obtained at a 13.3-nm-thick Al_2O_3 layer. We further modulate the thickness of the Al_2O_3 layer in order to explore the tunneling mechanism for the photocarriers. It is noticed that the dark current suffers more suppression with the increase of the thickness of the tunneling layer, while it hampers the photoresponsivity in the meantime. Therefore, the thickness should be properly optimized and balanced to enhance the performance. In addition, different from TMDCs that rely on the electron beam lithography (EBL) and mechanical exfoliation alignment process, the fabrication is compatible with the conventional semiconductor process that adopts Al_2O_3 as a tunneling layer and silicon as a photosensitive area, providing flexibility to future large-scale photodetectors with high integration.

2 Results and discussion

The detailed fabrication process of a Gr/Al_2O_3/Si tunneling photodetector is illustrated in the Supplementary Information (Figure S1), and the schematic diagram of a Gr/Al_2O_3/Si heterojunction photodetector is shown in Figure 1A. A 658 nm laser is illuminated on the bottom graphene of the heterostructure, and all the measurements are performed

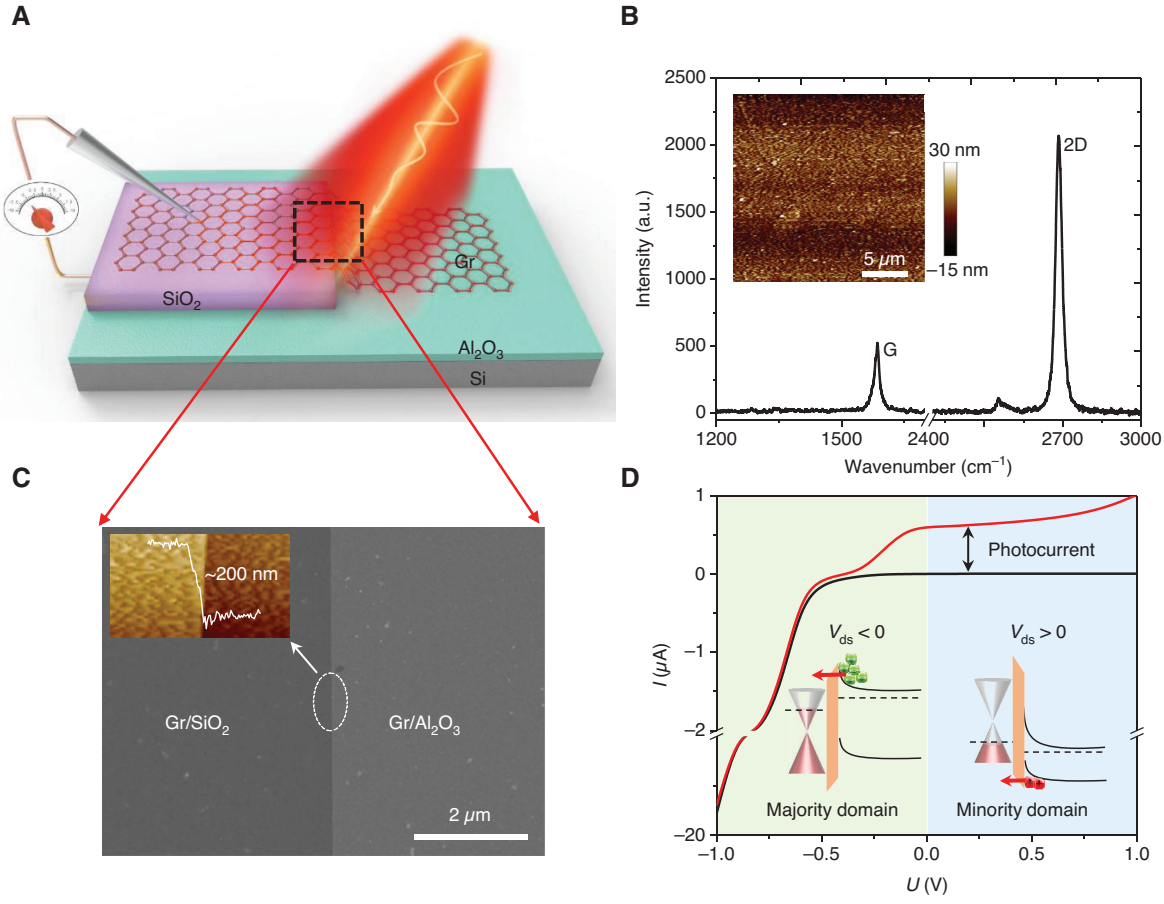

Figure 1: Schematic diagram and mechanism illustration of the Gr/Al_2O_3/Si heterojunction photodetector.
(A) Illustration of the Gr/Al_2O_3/Si heterojunction photodetector. Laser was illuminated on the bottom graphene of the device. (B) Raman spectrum of the graphene; inset: surface morphology of the Al_2O_3 tunneling layer. (C) SEM image of the graphene at the interface; inset: AFM image with height profile, indicating that the thickness of the top SiO_2 insulator is ~200 nm. (D) I/V curves of the Gr/Al_2O_3/Si photodetector under dark (black curve) and 658 nm laser illumination (red curve). The inset illustrates the energy band diagrams of the device at positive and negative bias voltage, respectively.

by applying a drain voltage on Si (terminal "d") with Gr being ground (terminal "s"). The thickness of the Al_2O_3 layer is measured by the ellipsometer (Supplementary material S2), with 4.91 nm, 13.36 nm and 21.12 nm, respectively. Furthermore, the Raman spectrum is performed to evaluate the quality of the bottom graphene, as shown in Figure 1B. It is observed that the G and 2D peaks can be clearly observed at 1587 and 2685 cm^{-1}, with a negligible D peak located at 1349 cm^{-1}. The 2D/G intensity ratio is around 2.2, indicating that the chemical vapor deposition grown graphene is mostly a monolayer. Also, the low intensity of the D peak demonstrates that few additional defects are generated during the transfer process. Figure 1C exhibits the scanning electron microscopy (SEM) image of the cross-sectional area, in which the different layers can be easily distinguished according to the contrast. The thickness of the top SiO_2 insulator is ~200 nm, shown in the atomic force microscopy (AFM) image with a height profile (inset). Considering a relatively high insulator layer, it is reasonable to determine the leakage current through the unilluminated area as negligible.

Figure 1D illustrates the current-voltage (I-V) curves of the Gr/Al_2O_3/Si photodetector under darkness and illumination ($P = 732$ μW, $\lambda = 658$ nm) with a 13.36-nm-thick tunneling layer. Similar to the Gr/Si Schottky photodetector, the photogenerated carriers still reside in the silicon while the graphene functions as the carrier collector in the tunneling heterojunction. Due to the photovoltaic effect, the built-in electric field separates the charges, showing conventional photodiode-like behavior. Furthermore, the current rectifying behavior can be understood by the inset, with the positive bias (minority domain mode) and the negative bias (majority domain mode), respectively. It is noticed that the measured current can be simplified as the sum of the tunnel current and photocurrent. With $V_{ds} < 0$, photoexcited electrons tunnel from silicon to graphene, whereas electrons are dominant in the n-type area that the photogenerated carriers cannot be competitive with the majority carriers ($I \approx I_{tunnel}$). Conversely, we can observe a clear current enhancement when $V_{ds} > 0$, as the recombination is governed by minority carriers (holes) that a similar amount of photogenerated and tunnel current is detected ($I = I_{tunnel} + I_{photogenerated}$). Meanwhile, many effects are ignored in the simplified mode such as the asymmetry tunneling process [22] or the Fermi level shift of graphene [4]. Nonetheless, we will show that the tunneling photodetector can demonstrate excellent photoresponse characteristics with this simple model (detailed experimental data in Figure 2).

To quantitatively investigate the photoresponse characteristics, the I-V curves under different illumination densities are measured and shown in Figure 2A, with the incident laser wavelength of 658 nm and the thickness of the Al_2O_3 layer of 13.36 nm. The photogenerated current is improved by two or three orders of magnitude compared with the dark current as V_{ds} varies from 0 V to 20 V. With increasing laser power, a stronger light-matter interaction can be achieved at the tunneling junction, which results in the enhancement of photogenerated minority carriers. Further increasing V_{ds}, however, a saturation tendency in the photocurrent can be observed. Also, the photocurrent can be defined as $I_{ph} = I_{illuminated} - I_{dark}$, and the measured data under different laser powers are illustrated in Figure 2B. The results are fitted with the equation $I_{ph} = aP^{\alpha}$, where I_{ph} is the photocurrent, a is a fitting parameter, P is the laser power intensity, α is an exponent and determines the response of the photocurrent to light intensity, and the values of a and α are 4.404×10^{-5} and 0.83, respectively. These values are associated with the recombination process of photogenerated carriers as well as the presence of some trap states between the Fermi level and the conduction band. With the obtained $\alpha = 0.83$, it is supposed that the energy loss during the recombination is relatively low for the tunneling heterojunction photodetector.

Moreover, the photoresponsivity (R) and detectivity (D^*) are generally utilized to evaluate the performance of a photodetector. Photoresponsivity is defined as $R = I_{ph}/P \cdot S$, where I_{ph} is the photocurrent, P is the incident light power density and S is the effective area under illumination. Short noise is the major contributor to the total noise [23], so that detectivity can be calculated by the equation $D^* = R \cdot S^{1/2}/(2e \cdot I_{dark})^{1/2}$, where R is the responsivity, e is the electronic charge and I_{dark} represents the dark current. The responsivity and detectivity of this device (13.3-nm-thick Al_2O_3 layer) increase with increasing V_{ds}, and the maximum values can reach up to 0.75 A/W and 3.1×10^{12} Jones (Figure 2C), respectively. Figure 2D shows R and D^* along with various illumination densities at $V_{ds} = 20$ V. It is noticed that both responsivity and detectivity basically remain unchanged with increasing illumination density. Besides, the I_{ph}/I_{dark} ratio is found to increase gradually with increasing light intensity and bias voltage, reaching up to as high as 4.8×10^3 when the light intensity is 1204 μW/cm^2 and V_{ds} is 22 V. Meanwhile, further increasing V_{ds} will also aggrandize the dark current and the photo-induced carriers become saturated, which hampers the I_{ph}/I_{dark} ratio as well as photoresponsivity and detectivity.

In order to explain these experimental results, we resort to a basic tunneling model and semiconductor theory. For a conventional Si-Gr structure, the photogenerated carriers are free to transport through the interface in the absence of an oxide barrier [4, 24]. However, with

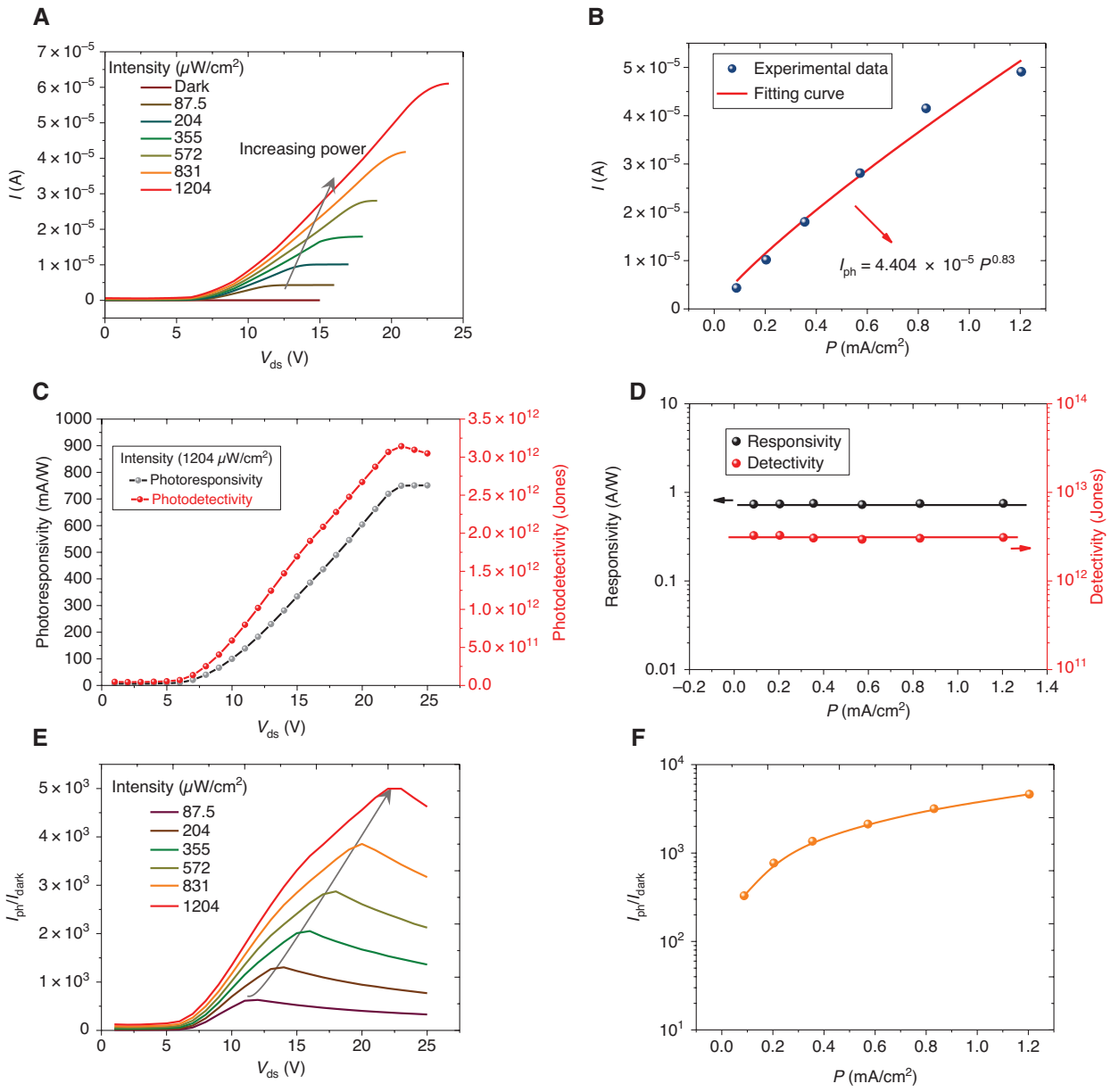

Figure 2: Photoresponse characteristics of the Gr/Al_2O_3/Si heterojunction photodetector.
(A) I-V curves under different illumination densities. Incident laser is 658 nm and the thickness of the Al_2O_3 layer is 13.36 nm. (B) Dependence of photocurrent on illumination power intensities. (C), (D) Photoresponsivity and photodetectivity with various V_{ds} and illumination power intensities, respectively. (E), (F) I_{ph}/I_{dark} ratio as a function of V_{ds} and illumination power intensities, respectively.

an oxide barrier or tunneling layer, the photogenerated carriers will accumulate at the silicon-oxide interface at low voltage [19]. Afterwards, the increasing bias voltage will compress the potential barrier and push it towards the junction. The I-V curves above can be modeled by the Fowler-Nordheim (F-N) tunneling theory, expressed by the following equation [25, 26]:

$$I_{FN}(V) \propto V_{ds}^2 \exp\left(-\frac{8\pi d\sqrt{2m^*\varphi}}{3heV_{ds}}\right) \quad (1)$$

where d, m^*, φ and h are the tunneling thickness (Al_2O_3 in this case), effective electron mass, tunneling barrier, and the Plank constant, respectively. By taking the logarithm of both sides, Eq. (1) becomes [27, 28]

$$\ln\frac{I_{FN}(V)}{V_{ds}} \propto -\frac{8\pi d\sqrt{2m^*\varphi}}{3heV_{ds}} \quad (2)$$

Based on Eq. (2), the plot of $\ln(I/V_{ds})$ versus V_{ds}^{-1} of the I-V curve is depicted in Figure 3A, with the light intensity

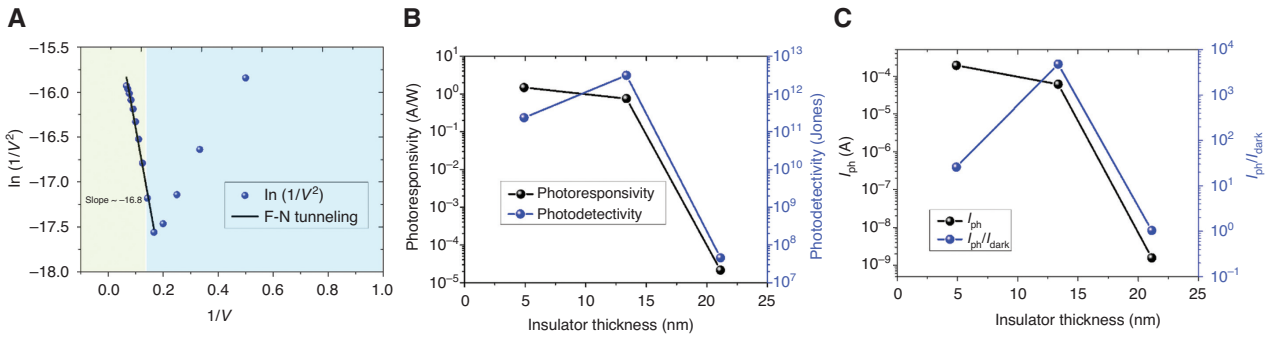

Figure 3: F-N fitting for the photoresponse characteristics, with the dependence of photoresponsivity and photodetectivity for different insulator thicknesses.

(A) $\ln(I(V)/V^2) - 1/V$ curve and Fowler-Nordheim fitting in the positive drain voltage regime. (B) Dependence of photoresponsivity and photodetectivity with different Al_2O_3 thicknesses. The thickness of the tunneling layer is 4.91 nm, 13.36 nm and 21.12 nm, respectively. (C) The photocurrent and I_{ph}/I_{dark} ratio with respect to Al_2O_3 thicknesses.

of 1204 μW/cm². It is clearly observed that the plot shows a linear tendency with the negative slope for F-N tunneling. To verify this tunneling process, we further modulate the thickness of Al_2O_3 and characterize the photoresponse performance. Figure S3 shows the I-V curves under different illumination densities, with 4.91-nm- and 21.12-nm-thick tunneling layers, respectively. We can find that the corresponding plots of $\ln(I/V_{ds})$ versus V_{ds}^{-1} demonstrate linearity in high voltage, while the calculated negative slopes decrease with increasing insulator thickness. For the conventional F-N emission or the so-called field emission [29, 30], the negative slopes are defined as the field enhancement factor β, which reveals the capability of the electric field motivating the electron tunneling from the emitters [31]. In this case, the value of the negative slope can be considered as the capacity of photogenerated carriers tunneling through the heterojunction as well as the recombination at the interface.

Figures 3B,C show the dependence of R, D^*, I_{ph} and the I_{ph}/I_{dark} ratio on different Al_2O_3 thicknesses. The thickness of the tunneling layer is 4.91 nm, 13.36 nm and 21.12 nm, respectively. According to $J \propto \exp(\xi^{1/2}d)$ (ξ is the tunneling barrier height of the insulator layer in eV and d is the insulator thickness) [32], the tunneling current ought to decrease with increasing thickness of Al_2O_3, which is consistent with the experimental results. As a result, the variation trend of R and I_{ph} is just the same as the tendency reflected in the Al_2O_3 thicknesses. However, we notice that the dark current suffers more suppression with the increase in the thickness of the tunneling layer, while it hampers the photoresponsivity in the meantime. With a thin insulator layer ~4.91 nm, a large photocurrent and photoresponsivity (1.99 A/W) ought to be acquired, while the carriers in Gr and silicon can also easily tunnel through the thin Al_2O_3 layer, which leads to a high dark current and low I_{ph}/I_{dark} ratio as well. On the other hand, for a 21.12-nm-thick Al_2O_3 layer, both photocurrent and dark current are suppressed as the thick insulator layer raises the difficulty for carrier tunneling. The band diagram of the heterojunction can be deduced from the photoresponse characteristics, as shown in Figure S4 with a simple triangle barrier model. At the forward bias, the tunneling probability through the insulator layer is exponentially decreased with increasing insulator thickness [33]. Therefore, unlike photocurrent and responsivity, the thickness of the tunneling layer should not only be thin enough to allow the photo-induced carriers to transport through the heterojunction, but also sufficient to limit the dark current, thereby obtaining the optimized D^* and I_{ph}/I_{dark} ratio.

Response speed can reflect the capability of a photodetector following the rapid optical signal. Figure 4 shows the photoresponse time measurement of the $Gr/Al_2O_3/Si$ tunneling photodetector in this study. By turning on and off the laser light with a chopper at 0.1 Hz, the photodetector exhibits excellent stability with various illumination densities, as shown in Figure 4A. Furthermore, a high-speed oscilloscope is utilized to measure the rapid optical signal generated by a laser diode driven by a function generator. Here the rise/fall time is defined as the photocurrent increased/decreased from 10/90% to 90/10% of the stable photocurrent. It is noted that the rise and fall time is 2.8 ms and 3.6 ms, respectively. In addition, the fast photoresponse measurements under pulse illumination with frequencies of 50 Hz, 100 Hz, 500 Hz and 1 kHz are depicted in Figure S5, respectively. Under periodic on/off illumination, our device can demonstrate switching performance with fast photoresponse and good reproducibility for frequencies of 50 Hz, 100 Hz and 500 Hz. As the frequency reaches up to 1 kHz, however, the photodetector is not perfectly recovered when the light is off. Without illumination, the generation of photo-induced carriers is stopped while residual photogenerated carriers still

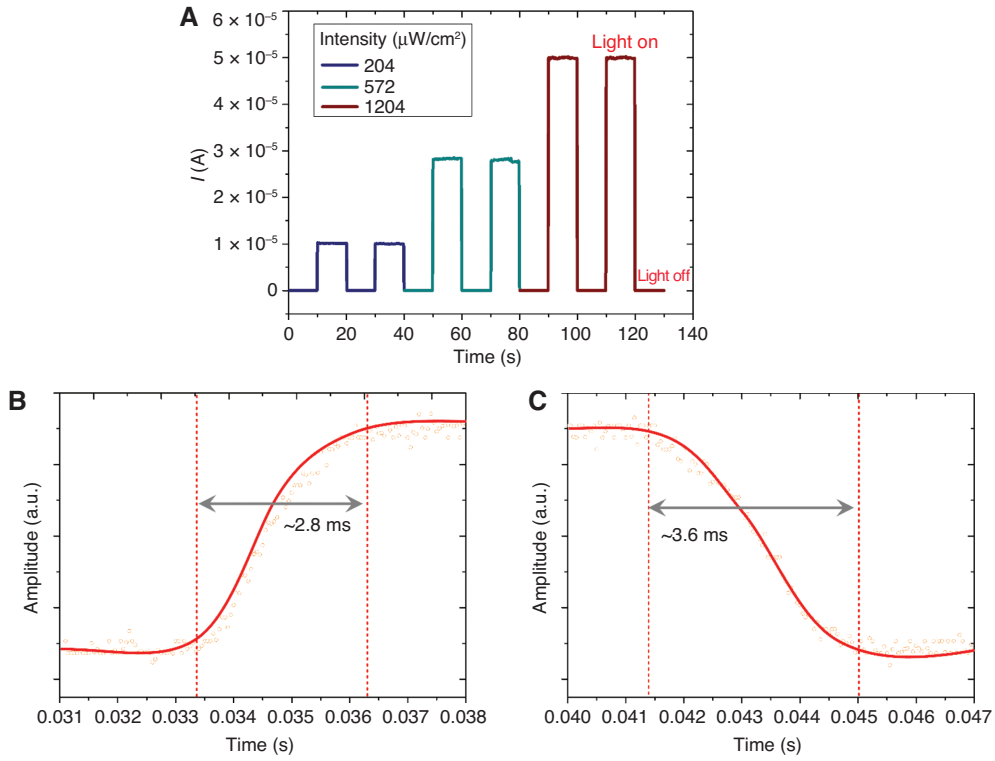

Figure 4: Photoresponse time measurement of the Gr/Al_2O_3/Si heterojunction photodetector.
(A) Photocurrent response of the photodetector with various illumination densities; the laser light is turned on/off by a chopper at 0.1 Hz. (B, C) Show the rise time and fall time of the photocurrent temporal response, respectively. Here the rise/fall time is defined as the photocurrent increased/decreased from 10/90% to 90/10% of the stable photocurrent.

transferred through the heterojunction or recombined at the interface because of the photovoltaic effect. It is worth noting that the response time of our device is not inferior to the reported tunneling photodetectors based on 2D TMDCs (Table 1). However, the response time of photovoltaic-type tunneling photodetectors is much slower than that of other TMDCs-based hybrid photodetectors, which is related to the built-in electric field and electronic properties of light-sensitive materials. We believe that optimization of quality of the 2D materials or insulator thickness may obtain short transit time of photogenerated carriers across the channel, enhancing the photoresponse characteristics eventually.

Table 1 shows the photoresponse performance of heterojunction tunneling photodetectors, based on different 2D materials and tunneling mechanisms [20, 21, 23, 34–37]. In the reported photovoltaic-type devices, photo-induced electron-hole pairs are separated by the built-in electric field, while the carrier tunneling follows different mechanisms. Photodiodes based on Gr, MoS_2 or $MoTe_2$ have been reported, and most of them are in good accordance with direct tunneling (DT) and F-N tunneling. With the insulator acting as the tunneling layer, e.g. hexagonal boron nitride (h-BN), DT occurs at low voltage and the carriers are dominated by F-N tunneling

Table 1: Comparison of 2D materials-based tunneling photodetectors with different tunneling mechanisms.

Device	Responsivity (A/W)	I_{ph}/I_{dark} ratio	Calculated detectivity (Jones)	Rise time (ms)	Tunneling mechanism	Ref
MoS_2/h-BN/Gr	3×10^{-4}	6.6		10		[20]
Gr/h-BN/$MoTe_2$	610		3.3×10^{11}	0.33	F-N tunneling	[34]
WSe_2/BP/MoS_2	6.32	400	1.25×10^{11}		Interband tunneling	[35]
MoS_2/h-BN/Gr	180	~10^5	2.6×10^{13}	230	DT and F-N tunneling	[21]
MoS_2/Gr/WSe_2	4250		2.2×10^{13}		Interband tunneling	[23]
Gr/MoS_2/Gr	0.068				DT tunneling	[36]
$SnSe_2$/BP	2.4×10^{-4}				Interband tunneling	[37]
Gr/Al_2O_3/Si	0.75	4.8×10^3	3.1×10^{12}	2.8	F-N tunneling	This paper

in the high-voltage regime [21]. Park et al. demonstrated a Gr/h-BN/$MoTe_2$ heterostructure, showing excellent photoelectric performance with a responsivity of 610 A/W and a rise time of 0.33 ms [34]. Yu and co-workers illustrated a highly sensitive photodetector with a MoS_2/h-BN/graphene heterostructure. The device can achieve a high photocurrent/dark current ratio of ~10^5, a responsivity of 180 A/W and an ultrahigh detectivity of 2.6×10^{13} Jones, which is about 100–1000 times higher than those of previously reported MoS_2-based devices [21]. All these reports found that the embedded h-BN barrier in vertical stacks can dramatically reduce dark current and increase detectivity for photodetector application.

Meanwhile, for the sandwich structure that is entirely composed of 2D materials, as the high electric field leads to the band bending at the atomically thin interface, carriers can tunnel through the valence band of the source (emitter) to the conduction band of the drain (collector), known as interband tunneling or band-to-band tunneling [38]. Similarly, dark carriers can also be compressed by combining various 2D materials as the tunneling layer, because of the large barrier potential difference in the heterojunction. Xu and co-workers first reported a photodetector based on a WSe_2/BP/MoS_2 van der Waals heterostructure, with a responsivity of 6.32 A/W and a detectivity of 1.25×10^{11} Jones, indicating its unique merit of photocurrent amplification capacity [35]. Miao et al. presented a sandwich structure by inserting graphene in an atomically thin p-n junction, and the MoS_2/Gr/WSe_2 heterojunction was successfully demonstrated for broadband photodetection in the visible to short-wavelength infrared range at room temperature [23].

For a further comparison between our photodetector and other 2D material-based devices, the photoelectric properties of responsivity, I_{ph}/I_{dark} ratio, detectivity and rise time of our device are also listed in Table 1. Under the illumination of 658 nm light, a responsivity of 0.75 A/W, a high current ratio of 4.8×10^3, a detectivity of 3.1×10^{12} Jones and a rise time of 2.3 ms have been obtained with the 13.3-nm-thick Al_2O_3 tunneling layer. We note that our Gr/Al_2O_3/Si tunneling photodetector can achieve comparable or even preferable values for the I_{ph}/I_{dark} ratio, detectivity and rise time, while the photoresponsivity is inferior to most TMDCs-based devices. However, it is well known that TMDCs rely heavily on the EBL and mechanical exfoliation alignment process, and that the high cost and difficulty in high integration restrict their practical applications in the industry. In the meantime, the fabrication of our device is compatible with the conventional semiconductor process that adopts Al_2O_3 as a tunneling layer and silicon as a photosensitive area, providing further flexibility to large-scale photodetectors with high integration.

3 Conclusions

In summary, by introducing Al_2O_3 as a tunneling layer between a silicon photoabsorber and a graphene electrode, a hybrid graphene/Al_2O_3/silicon tunneling photodetector is demonstrated as a high-performance photodetector. A maximum value of responsivity of ~0.75 A/W, a current ratio ~4.8×10^3 and a detectivity of ~3.1×10^{12} Jones have been obtained. The thickness of the Al_2O_3 layer is also modulated to explore the photoresponse characteristics and tunneling mechanism. It is noticed that the dark current suffers more suppression with the increase of tunneling layer, while it hampers the photoresponsivity in the meantime. Therefore, the thickness should be properly optimized and balanced to enhance the performance. In addition, the proposed graphene/Al_2O_3/silicon heterojunction device can be highly compatible with the conventional semiconductor process, which possesses huge potential in future optoelectronics and photovoltaic applications.

Acknowledgments: This work is financially supported by the China Postdoctoral Science Foundation (2019M651646), the National Natural Science Foundation of China (61904029, 61571124, 51902065, Funder Id: http://dx.doi.org/10.13039/501100001809), and the Beijing Municipal Natural Science Foundation (20B20253, Funder Id: http://kw.beijing.gov.cn/art/2019/11/20/art_1462_440954.html).

References

[1] Mueller T, Xia F, Avouris P. Graphene photodetectors for high-speed optical communications. Nat Photon 2010;4:297–301.
[2] Lemme MC, Koppens FHL, Falk AL, et al. Gate-activated photoresponse in a graphene p–n junction. Nano Lett 2011;11:4134–7.
[3] Gan X, Shiue R-J, Gao Y, et al. Chip-integrated ultrafast graphene photodetector with high responsivity. Nat Photon 2013;7:883–7.
[4] An X, Liu F, Jung YJ, Kar S. Tunable graphene-silicon heterojunctions for ultrasensitive photodetection. Nano Lett 2013;13:909–16.
[5] Xu X, Gabor NM, Alden JS, van der Zande AM, McEuen PL. Photothermoelectric effect at a graphene interface junction. Nano Lett 2010;10:562–6.
[6] Gabor NM, Song JCW, Ma Q, et al. Hot carrier-assisted intrinsic photoresponse in graphene. Science 2011;334:648–52.
[7] Liu C-H, Dissanayake NM, Lee S, Lee K, Zhong Z. Evidence for extraction of photoexcited hot carriers from graphene. ACS Nano 2012;6:7172–6.

[8] Nair RR, Blake P, Grigorenko AN, et al. Fine structure constant defines visual transparency of graphene. Science 2008;320:1308.
[9] Konstantatos G, Badioli M, Gaudreau L, et al. Hybrid graphene-quantum dot phototransistors with ultrahigh gain. Nat Nanotechnol 2012;7:363–8.
[10] Sun ZH, Liu ZK, Li JH, et al. Infrared photodetectors based on CVD-grown graphene and PbS quantum dots with ultrahigh responsivity. Adv Mater 2012;24:5878–83.
[11] Echtermeyer TJ, Britnell L, Jasnos PK, et al. Strong plasmonic enhancement of photovoltage in graphene. Nat Commun 2011;2:458.
[12] Fan YC, Shen NH, Zhang FL, et al. Two-dimensional optics: graphene plasmonics: a platform for 2D optics. Adv Opt Mater 2019;7:1800537.
[13] Shiue RJ, Gao YD, Wang YF, et al. High-responsivity graphene–boron nitride photodetector and autocorrelator in a silicon photonic integrated circuit. Nano Lett 2015;15:7288–93.
[14] Wei X, Yan FG, Lv QS, Shen C, Wang KY. Fast gate-tunable photodetection in the graphene sandwiched WSe_2/GaSe heterojunctions. Nanoscale 2017;9:8388–92.
[15] Lu JT, Wei AX, Zhao Y, et al. Graphene/In_2S_3 van der waals heterostructure for ultrasensitive photodetection. ACS Photon 2018;5:4912–9.
[16] Zhou X, Hu XZ, Zhou SS, et al. Tunneling diode based on WSe_2/SnS_2 heterostructure incorporating high detectivity and responsivity. Adv Mater 2018;30:1703286.
[17] Deng WJ, Chen YF, You CY, et al. Visible-infrared dual-mode MoS_2-graphene-MoS_2 phototransistor with high ratio of the I_{ph}/I_{dark}. 2D Mater 2018;5:045027.
[18] Yu XC, Li YY, Hu XN, et al. Narrow bandgap oxide nanoparticles coupled with graphene for high performance mid-infrared photodetection. Nat Commun 2018;9:4299.
[19] Liu CH, Chang YC, Norris TB, Zhong ZH. Graphene photodetectors with ultra-broadband and high responsivity at room temperature. Nat Nanotechnol 2014;9:273–8.
[20] Jeong H, Oh HM, Bang S, et al. Metal–insulator–semiconductor diode consisting of two-dimensional nanomaterials. Nano Lett 2016;16:1858–62.
[21] Vu QA, Lee JH, Nguyen VL, et al. Tuning carrier tunneling in van der Waals heterostructures for ultrahigh detectivity. Nano Lett 2017;17:453–9.
[22] Ng KK, Card HC. Asymmetry in the SiO_2 tunneling barriers to electrons and holes. J Appl Phys 1980;51:2153–7.
[23] Long MS, Liu EF, Wang P, et al. Broadband photovoltaic detectors based on an atomically thin heterostructure. Nano Lett 2016;16:2254–9.
[24] Chen C-C, Aykol M, Chang C-C, Levi AFJ, Cronin SB. Graphene-silicon Schottky diodes. Nano Letters 2011;11:1863–7.
[25] Lenzlinger M, Snow EH. Fowler-Nordheim tunneling into thermally grown SiO_2. J Appl Phys 1969;40:278.
[26] Simmons JG. Generalized formula for the electric tunnel effect between similar electrodes separated by a thin insulating film. J Appl Phys 1963;34:1793.
[27] Lee G-H, Yu Y-J, Lee C, et al. Electron tunneling through atomically flat and ultrathin hexagonal boron nitride. Appl Phys Lett 2011;99:243114.
[28] Ma Q, Andersen TI, Nair NL, et al. Tuning ultrafast electron thermalization pathways in a van der Waals heterostructure. Nat Phys 2016;12:455–9.
[29] Wu Z-S, Pei S, Ren W, et al. Field emission of single-layer graphene films prepared by electrophoretic deposition. Adv Mater 2009;21:1756–60.
[30] Di Bartolomeo A, Urban F, Passacantando M, et al. A WSe_2 vertical field emission transistor. Nanoscale 2019;11:1538–48.
[31] Kashid RV, Late DJ, Chou SS, et al. Enhanced field-emission behavior of layered MoS_2 sheets. Small 2013;9:2730–4.
[32] Park HK, Choi JW. Overlayer induced air gap acting as a responsivity amplifier for majority carrier graphene-insulator-silicon photodetectors. J Mater Chem C 2018;6:6958–65.
[33] Ning TH, Osburn CM, Yu HN. Emission probability of electrons from silicon into silicon oxide. J Appl Phys 1977;48:286–93.
[34] Heo J, Jeong H, Cho Y, et al. Reconfigurable van der Waals heterostructured devices with metal–insulator transition. Nano Lett 2016;16:6746–54.
[35] Li H, Ye L, Xu JB. High-performance broadband floating-base bipolar phototransistor based on WSe_2/BP/MoS_2 heterostructure. ACS Photon 2017;4:823–9.
[36] Yu WJ, Vu QA, Oh H, et al. Unusually efficient photocurrent extraction in monolayer van der Waals heterostructure by tunnelling through discretized barriers. Nat Commun 2016;7:13278.
[37] Yan RS, Fathipour S, Han YM, et al. Esaki diodes in van der Waals heterojunctions with broken-gap energy band alignment. Nano Letters 2015;15:5791–8.
[38] Roy T, Tosun M, Cao X, et al. Dual-gated MoS_2/WSe_2 van der Waals tunnel diodes and transistors. ACS Nano 2015;9:2071–9.

Supplementary Material: The online version of this article offers supplementary material (https://doi.org/10.1515/nanoph-2019-0499).